

Nanoscale

Accepted Manuscript



This is an *Accepted Manuscript*, which has been through the Royal Society of Chemistry peer review process and has been accepted for publication.

Accepted Manuscripts are published online shortly after acceptance, before technical editing, formatting and proof reading. Using this free service, authors can make their results available to the community, in citable form, before we publish the edited article. We will replace this *Accepted Manuscript* with the edited and formatted *Advance Article* as soon as it is available.

You can find more information about *Accepted Manuscripts* in the [Information for Authors](#).

Please note that technical editing may introduce minor changes to the text and/or graphics, which may alter content. The journal's standard [Terms & Conditions](#) and the [Ethical guidelines](#) still apply. In no event shall the Royal Society of Chemistry be held responsible for any errors or omissions in this *Accepted Manuscript* or any consequences arising from the use of any information it contains.

Pre-lithiation of onion-like carbon/MoS₂ nano-urchin anodes for high-performance rechargeable lithium ion batteries

Ye Wang¹, Guozhong Xing², Zhao Jun Han,³ Yumeng Shi,¹ Jen It Wong,¹ Zhi Xiang Huang,¹ Kostya (Ken) Ostrikov,^{3,4,5} Hui Ying Yang^{1*}

¹ Pillar of Engineering Product Development, Singapore University of Technology and Design, 20 Dover Drive, 138682, Singapore

² School of Materials Science and Engineering, The University of New South Wales, Sydney, New South Wales 2052, Australia

³ CSIRO Materials Science and Engineering, P.O. Box 218, Lindfield, New South Wales 2070, Australia

⁴ School of Chemistry, Physics, and Mechanical Engineering, Queensland University of Technology, Brisbane, Queensland 4000, Australia

⁵ School of Physics, The University of Sydney, New South Wales 2006, Australia

* Corresponding author. Tel.: +65 6303 6663; Fax: +65 6779 5161.
E-mail address: yanghuiying@sutd.edu.sg (H. Y. Yang)

Abstract

Hybrid urchin-like nanostructures composed of spherical onion-like carbon (OLC) core and MoS₂ nanoleaf were synthesized by a simple solvothermal method followed by thermal annealing treatment. Compared to the commercial MoS₂ powder, MoS₂/OLC nanocomposites exhibit enhanced electrochemical performance as the anode material of lithium-ion batteries (LIBs) with a specific capacity of 832 mAh g⁻¹ at the current density of 50 mA g⁻¹ after 60 cycles, and a moderate initial Coulombic efficiency of 71.1%. Furthermore, a simple pre-lithiation method based on a direct contact of a lithium foil with the MoS₂/OLC nano-urchins was used to achieve a very high Coulombic efficiency of 97.6% in the first discharge/charge cycle, which is at least 26% higher compared to pristine MoS₂/OLC nano-urchins. This pre-lithiation method can be generalized to develop other carbon-metal sulfide nanohybrids for LIB anode materials. These results may open up a new avenue for the development of the next-generation high-performance LIBs.

Keywords: onion-like carbon, MoS₂; lithium-ion batteries; pre-lithiation; nano-urchins, initial Coulombic efficiency.

Introduction

High-performance rechargeable lithium-ion batteries (LIBs) are highly desirable for modern portable electronic devices and hybrid electrical vehicles (HEVs).^{1,2} LIBs attract rapidly increasing research and industry interests due to their high energy density, long cycle stability and no memory effect compared to other alternatives.³⁻⁷ Currently, commercial LIBs employ graphite as the anode material, which possesses a relative low theoretical specific capacity ($\sim 372 \text{ mAh g}^{-1}$).^{8,9} To enhance the performance, nano-sized metal oxides with very high theoretical capacity and shortened lithium ion diffusion lengths have been extensively investigated for applications as LIBs anode materials.¹⁰⁻¹⁶ However, the large volume change during the lithiation and de-lithiation processes and the relative low conductivity of metal oxides lead to poor cycling stability and rate capability, which negatively affects their commercialization prospects.^{17, 18} Moreover, most of the anode materials suffer from low initial Coulombic efficiency (CE) due to the irreversible capacity loss during the first charge/discharge cycle.

Recently, nano-structured layered transition metal dichalcogenide (LTMD) materials such as MoS_2 have been investigated as anode materials of LIBs owing to their prominent advantages.¹⁹⁻²¹ First, due to the layered structure, the weak van der Waals interactions between MoS_2 layers makes it possible to insert and then extract Li ions without a significant volume change.²² This prevents the common pulverization problem in metal oxides or other alloy-type anode materials. Second, the theoretical specific capacity $\sim 670 \text{ mAh g}^{-1}$ of MoS_2 (based on the conversion reaction between Li ions and MoS_2 resulting in four moles of lithium incorporation per mole of MoS_2) is much higher compared to commercial graphite.²³ It has been demonstrated that integration of MoS_2 with

carbonaceous materials (*e.g.*, carbon nanotubes (CNTs), graphene oxide, mesoporous carbon, and templated graphite) enhances electrochemical performance.²⁴⁻³⁰ For example, coaxial MoS₂/CNTs nanostructures exhibited a capacity of 400 mAh g⁻¹;³¹ MoS₂/graphene nanohybrids showed a capacity of 1187 mAh g⁻¹ after 100 cycles;³² Furthermore, hierarchical MoS_x/CNT (2<x<3) nanocomposites also showed a high capacity of >1000 mAh g⁻¹ at a current density of 50 mA g⁻¹, as well as long cycle stability.²² However, in the previous studies the initial CE of anode materials remained relatively low, *i.e.*, between 65 to 75%.

Higher CE values are sought to increase the discharging capacity relative to the charging capacity. However, a large number of lithium ions are trapped into a solid-electrolyte interface (SEI) layer that forms during the first lithiation process, leading to low initial CE values. This amount of lithium ions are provided by cathode electrode in secondary LIBs, resulting in redundant cathode used and high cost. A pre-lithiation process has been proposed to compensate the loss of lithium ions during the initial lithiation process.³³ Such pre-lithiation method has been widely used for lithium sulfur battery, and cathode material of LIBs, but is not common for LIBs anode materials due to the instability of the lithiated materials and process complexity.³⁴ Several prelithiation methods have been developed, including chemical reaction with *n*-butyllithium, electrochemical prelithiation, as well as hydrothermal treatment with LiCl and stabilized lithium metal powder (SLMP).^{33, 35-37} Recently, it has been demonstrated that pre-lithiation can be achieved by placing a Li foil contacting with the material to be lithiated, such as silicon nanowires.³⁴ Compared to other methods, this pre-lithiation technique showed several advantages of easy operation, low cost, and high lithiation efficiency.

Here we report on MoS₂/onion-like carbon (OLC) nano-urchins by growing MoS₂ nanoleaves with spherical OLC using a simple solvothermal method followed by thermal annealing treatment. The MoS₂/OLC nano-urchins were employed as the anode material for LIBs and exhibit much improved specific capacity and cycle stability. Furthermore, a pre-lithiation method was implemented on the MoS₂/OLC nano-urchins and the corresponding initial CE is improved greatly from 71.1% to 97.6% with excellent reaction reversibility.

Experimental

Materials synthesis

MoS₂/OLC nano-urchins were synthesized *via* a simple single-step solvothermal method. Briefly, 220 mg (NH₄)₂MoS₄ powder and 10 mg OLC were mixed and thoroughly dispersed into 30 ml N,N-dimethylformamide (DMF) by probe sonication and continuous stirring for about 15 min at room temperature.²² After that, the precursor was transferred to a 50 ml Teflon-lined stainless steel autoclave, sealed and kept in a normal lab oven at 200 °C for 10 h. The product was collected by centrifugation and washed by de-ionised water for several times to remove unreacted chemicals and DMF residue. After drying the product at 100 °C overnight in a vacuum oven, the final powder was annealed at 500 °C for 2 h in the Ar gas flow to remove the sulfur residue.

Prelithiation process

The prelithiation process was implemented by directly contacting MoS₂/OLC active material with lithium foil in a CR2032 coin cell setup. The MoS₂/OLC slurry was

prepared by dispersing 80 wt% MoS₂/OLC, 10 wt% conductive carbon black and 10 wt% polyvinylidene difluoride (PVDF) binder in N-methylpyrrolidone (NMP). The slurry was then painted onto nickel foam and dried overnight in a vacuum oven at 120 °C. The prepared electrode covered with a lithium foil was assembled into a standard CR2032 button cell and filled with 1 M LiPF₆ solution dissolved in a mixture of ethylene-carbonate–ethyl-methyl-carbonate (EC–EMC, 1 : 1) as the electrolyte in an argon-filled glove box. The cell was then disassembled after the prelithiation for 24 hours.

Electrochemical measurements

The electrochemical performance of MoS₂/OLC nano-urchins and related pre-lithiated nanocomposites were measured by assembling them into a two-electrode half-cell configuration, with the active materials as the working electrode and a lithium foil as the counter electrode. The electrode fabrication and assembly processes were the same as that in the pre-lithiation process, except that Celgard 2400 membranes were used as the separators between the working and counter electrodes. Electrochemical measurements were carried out after 24 h of the assembly. The cyclic voltammetry (CV) and electrochemical impedance spectroscopy (EIS) measurements were achieved using an electrochemical workstation (VMP3, Bio-logic, France). The galvanostatic charge/discharge test was performed in the voltage range of 0.01-3 V at various current densities ranging from 50 to 2000 mA g⁻¹ by a battery analyzer (Neware, Shenzhen, China).

Materials characterization

The morphologies and structures of the samples were examined by field-emission scanning electron microscopy (FESEM, JSM-7600) and transmission electron microscopy (TEM, JEM-2100F). Crystal structure of the nano-urchins was investigated by X-ray diffraction (XRD, Siemens, D5005) with Cu K α ($\lambda=0.154$ nm) radiation under the accelerating voltage of 40 kV. Raman spectra were obtained by a confocal Raman system with the laser excitation at 532 nm (WITec Instruments Corp, Germany). The content of MoS₂ in the nanocomposites was examined by thermogravimetric analysis (TGA, Shimadzu, DTG-60). The chemical composition was investigated by X-ray photoelectron spectroscopy (XPS, Thermo Scientific, ESCA-Lab-250xi) using Al K α source ($h\nu =1486.68$ eV) in an UHV chamber at a pressure lower than 2.0×10^{-7} Pa. The peak positions were calibrated on the C 1s peak position at 285.0 eV.

Results and discussion

The morphology of the OLC and MoS₂/OLC nanocomposites is shown in Figure S1 and Figure 1, respectively. Pristine OLC shows a spherical morphology with a diameter of about 15-40 nm (Figure S1), while MoS₂/OLC nano-urchins feature a nanoporous spherical structure with a diameter of 40-80 nm and covered by numerous MoS₂ nanoleaves (Figure 1a). The MoS₂ nanoleaves can be distinguished from the TEM image in Figure 1b. The interplanar spacing of the MoS₂ sheets is 0.62 nm, corresponding to the (002) crystal plane.²⁴ In addition, the valence states and chemical composition in the MoS₂/OLC nano-urchins have been investigated by XPS, as shown in Figures 1c. The binding energy peaks located at 232.7, 229.6, 163.6 and 162.4 eV corresponded to Mo 3d_{3/2}, Mo 3d_{5/2}, S 2p_{1/2} and S 2p_{3/2} states, respectively. In particular, Mo atoms find

themselves in the 4+ valence state in the synthesized MoS₂/OLC nano-urchins, indicating the crystal structure is MoS₂.

The crystal structure of the synthesized MoS₂/OLC nano-urchins was examined by XRD, as shown in Figure 2a. A broad peak 2θ centered at 20° originates from the quartz substrate background and a weak peak at around 26° corresponds to the (002) plane of OLC.³⁸ Other diffraction peaks in this figure could be indexed as the (002), (100), (103) and (110) planes of the MoS₂ crystal (JCPDS No. 37-1492), in a good agreement with the previous reports.²⁴ The synthesized MoS₂/OLC nanocomposites were further analyzed by the Raman spectroscopy shown in Figure 2b. Two major Raman peaks located at 383 and 408 cm⁻¹ can be assigned to the typical Raman-active E_{2g}^1 and A_{1g} modes of MoS₂, respectively, and are also observed for commercial MoS₂ powder.³⁹ On the other hand, the peaks located at 1384 and 1592 cm⁻¹ are attributed to the D- and G-peaks corresponding to the disorder and defects in the carbon layer, and the in-plane vibration of sp²-bonded carbon atoms in the hexagonal carbon lattice, respectively.⁴⁰⁻⁴²

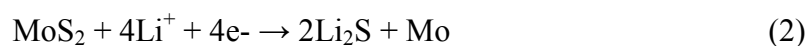
In order to determine the content of OLC in the nano-urchins, thermal gravimetric analyses (TGA) and differential scanning calorimetry (DSC) measurements were performed under oxygen atmosphere and the corresponding curves are shown in Figure S2. When the temperature is less than 100 °C, a small weight loss was observed due to the evaporation of moisture adsorbed on the surface of nanocomposites. As the temperature increased, a further weight loss of 35.3% between 100 and 380 °C was attributed to the carbon oxidization in air, which was associated with large amounts of heat released as seen in the DSC curve. A final weight loss of 8.23% was observed between 380 and 530 °C, corresponding to the oxidation reaction of MoS₂ to form

MoO₃.⁴³ Therefore, MoS₂/OLC nano-urchins contain 63.4 wt% of MoS₂ and 36.6 wt% of OLC.

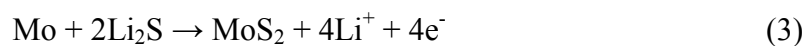
The electrochemical performance of the nanocomposites was evaluated by integrating them into a half-cell battery configuration composed of the active material as the working electrode and a lithium foil as the counter electrode. Figure 3a shows the CV curve of the first three cycles within the potential range of 0.01-3V vs Li/Li⁺. In the first cathodic cycle, there are two peaks centered at 1.15 and 0.58 V. The former corresponds to the lithium intercalation into MoS₂ layered lattice to form Li_xMoS₂, as described by the following equation.



It is worth mentioning that during the intercalation process, MoS₂ undergoes a first-order phase transition from the semiconducting 2H phase into the more electrically conductive 1T metastable phase, where the coordination of Mo atoms becomes octahedral.^{44, 45} On the other hand, the peak centered at 0.58 V is associated with the reduction of Mo²⁺ into the metallic Mo nanoparticles embedded into a Li₂S matrix through the conversion process (see equation 2) and the formation of a gel-like SEI layer at the interface of the electrolyte and the electrode.^{22, 46-48}



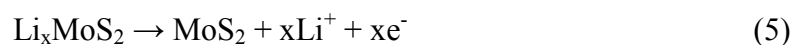
In the first anodic cycle, we observed a relatively weak peak located at 1.4 V and one main peak at 2.3 V, corresponding to the oxidation of Mo to MoS₂,^{22, 47}



and dissociation oxidation of Li_2S , respectively.⁴⁹



In the second cathodic CV cycle, a new redox peak associated with the reduction of S into Li_2S was found at 1.9 V and a broad peak associated with the lithium intercalation formation of Li_xMoS_2 at 1.12 V.^{22, 46} These reactions became reversible with the oxidation peaks at 1.42 and 2.24 V that correspond to the extraction of Li^+ from Li_xMoS_2 lattice (see equations 5), and the oxidation of Li_2S , respectively.⁴³



The galvanostatic discharge/charge test was carried out in the potential range of 0.01-3.0 V vs. Li/Li^+ at a current density of 50 mA g^{-1} , and the curves of the first 5 discharge/charge cycles are shown in Figure 3b. In the first discharge curve, there are two plateaus located at 1.3-1.1 V and 0.7-0.5 V. These two plateaus are usually ascribed to the formation of Li_xMoS_2 through lithium intercalation and the conversion of MoS_2 into metallic Mo facilitated by the formation of the SEI layer.^{22, 43} On the other hand, the MoS_2/OLC nano-urchins exhibit an obvious plateau in the potential range between 2.0 and 2.3 V in the first charge curve, corresponding to the oxidization of Li_2S into S.⁴⁶ These discharge/charge behaviors are consistent with the CV curves shown in Figure 3a. The specific capacity of the first discharge and charge cycle were 1434 and 1020 mAh g^{-1} , respectively, resulting in an initial CE of 71.1% calculated by:⁵⁰

$$\text{CE} = \frac{\text{Delithiation capacity}}{\text{Lithiation capacity}} \times 100\% = \frac{\text{Charge capacity}}{\text{Discharge capacity}} \times 100\% \quad (6)$$

The capacity loss of approximately 28.9% during the initial cycle can be attributed to the irreversible decomposition of the electrolyte and the formation of SEI film.¹² Similar phenomena have been observed in other nano-sized anode materials.^{12, 13, 51} During the second cycle, the discharge and charge capacity decreased to 1002 and 947 mAh g⁻¹, respectively, resulting in a much higher CE of 94.5%. CE was further increased to 98.5% in the 4th cycle and maintained above 98.5% for longer cycles.

The cycling performance of MoS₂/OLC nanocomposites is also shown in Figure 3c. MoS₂/OLC still can deliver a high capacity of 853 mAh g⁻¹ after 60 cycles. In contrast, the specific capacity of the commercial MoS₂ powder was only 158 mAh g⁻¹ after 100 cycles (Figure S3). The improved capacity and cycling stability of the MoS₂/OLC nano-urchins as compared to the commercial MoS₂ powder can be attributed to synergistic effect of MoS₂ and the addition of OLC. First, OLC has outstanding electronic behavior and higher conductivity to improve the electron transfer rate.^{12, 38} Second, OLC also can effectively inhibit the restacking of MoS₂ layered structure, resulting in improved electrochemical performance.⁴⁸

The rate capability of MoS₂/OLC nano-urchins at various current densities is shown in Figure 3d. The nanocomposites exhibit reversible capacities of 826, 653, 493, 341 and 248 mAh g⁻¹ at the current densities of 50, 200, 500, 1000 and 2000 mA g⁻¹, respectively. Remarkably, the capacity could recover to ~874 mAh g⁻¹ after the current density was adjusted from 2000 mA g⁻¹ to 50 mA g⁻¹. It is worth mentioning that the rate capacity of our MoS₂/OLC nano-urchins was comparable or better than the high-end values obtained recently from novel hybrid anodes.²² We believe that the good rate capability arises from the isotropic nanoporous structure and good electrical conductivity of the spherically-

shaped OLC nanoparticles. Since the lithium ions can be inserted into and extracted from the active materials from all the directions, it indeed leads to the enhanced ion accessibility and ion transport and eventually, the better rate capability.^{38, 52} A similar concept of designing the electrodes could also be found in the case of MesoCarbon MicroBeads (MCMB)-based materials, which generally show a higher capability as compared to the natural graphite.⁵³

To further explore the intrinsic electrochemical and kinetic mechanisms of the nanocomposites, the electrochemical impedance spectroscopy (EIS) was carried out after the first three cycles. Figure 4 shows the Nyquist plots (symbol) of the commercial MoS₂ and the synthesized MoS₂/OLC nano-urchins. A much smaller semi-circle at high frequencies was observed for the MoS₂/OLC nano-urchins as compared to that of the commercial MoS₂, implying a lower charge transfer resistance. To quantify the performance of the two materials, we used an equivalent circuit model as shown in the inset of Figure 4, where R_s represents the electrolyte resistance corresponding to the intercept of the semicircle at high frequency range; R_f and Q1 are the SEI layer resistance and the constant phase element (CPE), respectively, corresponding to the semicircle at high frequency range; R_{ct} and Q2 are the charge transfer resistance and related double layer capacitor, respectively, corresponding to the semicircle in high-middle frequency region; and W is Warburg impedance corresponding to the straight line in low frequency range related to the lithium-diffusion process.^{12, 54} The fitting results are summarized in Table 1, which clearly indicates that the charge transfer resistance of MoS₂/OLC (19.22 Ω) was dramatically reduced compared to the commercial MoS₂ (60.62 Ω).

As discussed above, the initial CE of our MoS₂/OLC nano-urchins was only 71.1%, implying that a large amount of lithium ions became inactive after the first discharge process. In the operational rechargeable LIBs, this portion of lithium ions would be provided by the cathode (*e.g.*, LiFePO₄, LiCoO₂, *etc.*). However, this approach requires large amounts of Li-based cathode materials which are very expensive and also undesirable for several other reasons. To tackle this issue, we adopted a pre-lithiation method to provide lithium ions to the anode in advance rather than extract from the cathode materials. The pre-lithiation process is illustrated in Figure 5a, where the MoS₂/OLC nano-urchins are in direct contact with a lithium foil. Lithium ions were then absorbed within the surface layer and/or intercalated into the MoS₂ layered structure (Figure 5b).

The electrochemical performance of the pre-lithiated MoS₂/OLC nano-urchins was then measured in a half-cell battery configuration. The CV curves of the first two cycles in the potential range of 0.01-3 V vs. Li/Li⁺ are shown in Figure 6a. Unlike the features observed in the pristine MoS₂/OLC nano-urchins, the pre-lithiated nano-urchins showed very similar shape and peak positions for the first and second discharge/charge cycles. The pre-lithiated MoS₂/OLC delivered capacities of 772 and 753 mAh g⁻¹ for the first discharge and charge cycle process, respectively. Here, pre-lithiation process and the first time charge were treated as the zero time of cycle. Although the discharge specific capacity was slightly lower than that of the pristine sample, the initial CE increased significantly from 71.1% to 97.6% after the pre-lithiation. Moreover, the specific capacity stayed at a high level of 721 mAh g⁻¹ even after 100 cycles. To our best knowledge, this represents the first report of pre-lithiation of MoS₂ with such a high initial CE, thereby

demonstrating that the pre-lithated MoS₂/OLC nano-urchins can indeed be a promising anode material for next-generation high-performance LIBs.

In addition, the prelithiation method shown here is that the active material electrode, regardless of its type and structure, was contacted with the lithium foil directly. The prelithiation setup is based on the general setup tested for the active material which also employs lithium foil as a lithium source. Therefore, the prelithiation method could also be possibly applied to carbon-metal sulfide nanohybrids and other active materials. It is worth mentioning that two simple additional experimental steps (assembling and disassembling) of effective prelithiation of the anode material may effectively resolve a major CE issue arising during the first operation cycles. The above two extra steps are very simple and straightforward. They are also can be simplified by putting the electrodes and lithium foil into CR2032 case without assembling; thereafter a load can be applied to the assembly to enable a reasonably long contact between the electrodes and the lithium foil. This is just one simple possibility and many other engineering solutions may be available to further improve the battery assembly. This advantage gives more space for further improving the initial CE of anode material and lowering the cost of LIBs. Nevertheless, further studies are needed for high-yield and large-scale applications of this emerging technology.

Conclusion

In summary, we have reported a proof-of-concept study based on a synthesis of MoS₂/OLC nano-urchins by a simple solvothermal method followed by thermal annealing for applications as the anode material of LIBs. The pristine MoS₂/OLC nano-

urchins delivered a specific capacity of 832 mAh g^{-1} at the current density of 50 mA g^{-1} with an initial CE of 71.1%. A pre-lithiation method based on placing the nano-urchins in direct contact with the lithium foil was then employed to increase the initial CE to 97.6%. The strategy of pre-lithiation is generic and can also be used for other carbonaceous materials hybridized with metal sulfides for high-performance LIBs.

Acknowledgement

This work was supported by SUTD research grant SUTD-ZJU/RES/04/2011. CSIRO's Science Leadership Program and the Australian Research Council (ARC) are gratefully acknowledged. ZJH and KO thank the support from the DECRA and Future Fellowships from the ARC.

References

1. C. Liu, F. Li, L. P. Ma and H. M. Cheng, *Adv. Mater.*, 2010, **22**, E28.
2. M. Armand and J. M. Tarascon, *Nature*, 2008, **451**, 652.
3. J. Cabana, L. Monconduit, D. Larcher and M. R. Palacin, *Adv. Mater.*, 2010, **22**, E170.
4. S. Megahed and B. Scrosati, *J. Power Sources*, 1994, **51**, 79.
5. M. Park, X. Zhang, M. Chung, G. B. Less and A. M. Sastry, *J. Power Sources*, 2010, **195**, 7904.
6. M. He, L. Yuan, X. Hu, W. Zhang, J. Shu and Y. Huang, *Nanoscale*, 2013, **5**, 3298.
7. X. Cui, C. Z. Zhang, R. Hao and Y. L. Hou, *Nanoscale*, 2011, **3**, 2118.
8. L. W. Ji, Z. Lin, M. Alcoutlabi and X. W. Zhang, *Eng. Environ. Sci.*, 2011, **4**, 2682.
9. W. Shi, X. Rui, J. Zhu and Q. Yan, *J. Phys. Chem. C*, 2012, **116**, 26685.
10. M. Reddy, G. Subba Rao and B. Chowdari, *Chem. Rev.*, 2013, **113**, 5364.
11. P. Poizot, S. Laruelle, S. Grugeon, L. Dupont and J. M. Tarascon, *Nature*, 2000, **407**, 496.
12. Y. Wang, Z. J. Han, S. F. Yu, R. R. Song, H. H. Song, K. K. Ostrikov and H. Y. Yang, *Carbon*, 2013, **64**, 230.
13. Y. Wang, F. Yan, S. W. Liu, A. Y. S. Tan, H. Song, X. W. Sun and H. Y. Yang, *J. Mater. Chem. A.*, 2013, **1**, 5212.
14. K. Ostrikov, E. Neyts and M. Meyyappan, *Adv. Phys.*, 2013, **62**, 113.
15. U. Cvelbar, K. Ostrikov, I. Levchenko, M. Mozetic and M. K. Sunkara, *Appl. Phys. Lett.*, 2009, **94**, 211502.
16. U. Cvelbar, Z. Chen, M. K. Sunkara and M. Mozetič, *Small*, 2008, **4**, 1610.
17. J. Y. Huang, L. Zhong, C. M. Wang, J. P. Sullivan, W. Xu, L. Q. Zhang, S. X. Mao, N. S. Hudak, X. H. Liu, A. Subramanian, H. Fan, L. Qi, A. Kushima and J. Li, *Science*, 2010, **330**, 1515.
18. L. Su, Y. Jing and Z. Zhou, *Nanoscale*, 2011, **3**, 3967.
19. H. Hwang, H. Kim and J. Cho, *Nano Lett.*, 2011, **11**, 4826.
20. S. Ding, D. Zhang, J. S. Chen and X. W. D. Lou, *Nanoscale*, 2012, **4**, 95.
21. T. Stephenson, Z. Li, B. Olsen and D. Mitlin, *Eng. Environ. Sci.*, 2014, **7**, 209.
22. Y. Shi, Y. Wang, J. I. Wong, A. Y. S. Tan, C.-L. Hsu, L.-J. Li, Y.-C. Lu and H. Y. Yang, *Sci. Rep.*, 2013, **3**, 2169.
23. U. K. Sen and S. Mitra, *ACS Appl. Mater. Interfaces*, 2013, **5**, 1240.
24. X. Zhou, L.-J. Wan and Y.-G. Guo, *Nanoscale*, 2012, **4**, 5868.
25. C. Lu, W.-W. Liu, H. Li and B. K. Tay, *Chem. Commun.*, 2014, **50**, 3338.
26. X. Cao, Y. Shi, W. Shi, X. Rui, Q. Yan, J. Kong and H. Zhang, *Small*, 2013, **9**, 3433.
27. C. Zhang, Z. Wang, Z. Guo and X. W. Lou, *ACS Appl. Mater. Interfaces*, 2012, **4**, 3765.
28. C. Zhang, H. B. Wu, Z. Guo and X. W. D. Lou, *Electrochem. Commun.*, 2012, **20**, 7.

29. L. Fei, Y. Xu, X. Wu, G. Chen, Y. Li, B. Li, S. Deng, S. Smirnov, H. Fan and H. Luo, *Nanoscale*, 2014, **6**, 3664.
30. C. Wang, W. Wan, Y. Huang, J.-T. Chen, H. Zhou and X. Zhang, *Nanoscale*, 2014, **6**, 5351.
31. Q. Wang and J. Li, *J. Phys. Chem. C*, 2007, **111**, 1675.
32. K. Chang and W. Chen, *ACS Nano*, 2011, **5**, 4720.
33. M. W. Forney, M. J. Ganter, J. W. Staub, R. D. Ridgley and B. J. Landi, *Nano Lett.*, 2013, **13**, 4158.
34. N. Liu, L. Hu, M. T. McDowell, A. Jackson and Y. Cui, *ACS nano*, 2011, **5**, 6487.
35. B. Garcia, M. Millet, J. Pereira-Ramos, N. Baffier and D. Bloch, *J. Power Sources*, 1999, **81**, 670.
36. B. J. Landi, M. J. Ganter, C. D. Cress, R. A. DiLeo and R. P. Raffaele, *Eng. Environ. Sci.*, 2009, **2**, 638.
37. L. Q. Mai, B. Hu, W. Chen, Y. Qi, C. Lao, R. Yang, Y. Dai and Z. L. Wang, *Adv. Mater.*, 2007, **19**, 3712.
38. Y. Wang, S. F. Yu, C. Y. Sun, T. J. Zhu and H. Y. Yang, *J. Mater. Chem.*, 2012, **22**, 17584.
39. H. Li, Q. Zhang, C. C. R. Yap, B. K. Tay, T. H. T. Edwin, A. Olivier and D. Baillargeat, *Adv. Funct. Mater.*, 2012, **22**, 1385.
40. A. Ferrari, J. Meyer, V. Scardaci, C. Casiraghi, M. Lazzeri, F. Mauri, S. Piscanec, D. Jiang, K. Novoselov and S. Roth, *Phys. Rev. Lett.*, 2006, **97**, 187401.
41. A. C. Ferrari, *Solid State Commun.*, 2007, **143**, 47.
42. Q. Cheng, E. Tam, S. Xu and K. K. Ostrikov, *Nanoscale*, 2010, **2**, 594.
43. Z. Wang, T. Chen, W. Chen, K. Chang, L. Ma, G. Huang, D. Chen and J. Y. Lee, *J. Mater. Chem. A.*, 2013, **1**, 2202.
44. M. Py and R. Haering, *Can. J. Phys.*, 1983, **61**, 76.
45. G. Eda, H. Yamaguchi, D. Voiry, T. Fujita, M. Chen and M. Chhowalla, *Nano Lett.*, 2011, **11**, 5111.
46. L. Yang, S. Wang, J. Mao, J. Deng, Q. Gao, Y. Tang and O. G. Schmidt, *Adv. Mater.*, 2013, **25**, 1180.
47. X. Fang, X. Yu, S. Liao, Y. Shi, Y.-S. Hu, Z. Wang, G. D. Stucky and L. Chen, *Microporous Mesoporous Mater.*, 2012, **151**, 418.
48. K. Chang and W. Chen, *J. Mater. Chem.*, 2011, **21**, 17175.
49. J. Xiao, X. Wang, X. Q. Yang, S. Xun, G. Liu, P. K. Koech, J. Liu and J. P. Lemmon, *Adv. Funct. Mater.*, 2011, **21**, 2840.
50. M. Thakur, S. L. Sinsabaugh, M. J. Isaacson, M. S. Wong and S. L. Biswal, *Sci. Rep.*, 2012, **2**, 795.
51. J. C. Guo, Q. Liu, C. S. Wang and M. R. Zachariah, *Adv. Funct. Mater.*, 2012, **22**, 803.
52. J. W. Fergus, *J. Power Sources*, 2010, **195**, 939.
53. M. Yoshio, H. Wang, K. Fukuda, T. Umeno, T. Abe and Z. Ogumi, *J. Mater. Chem.*, 2004, **14**, 1754.
54. S.-Y. Liu, J. Xie, Y.-X. Zheng, G.-S. Cao, T.-J. Zhu and X.-B. Zhao, *Electrochim. Acta*, 2012, **66**, 271.

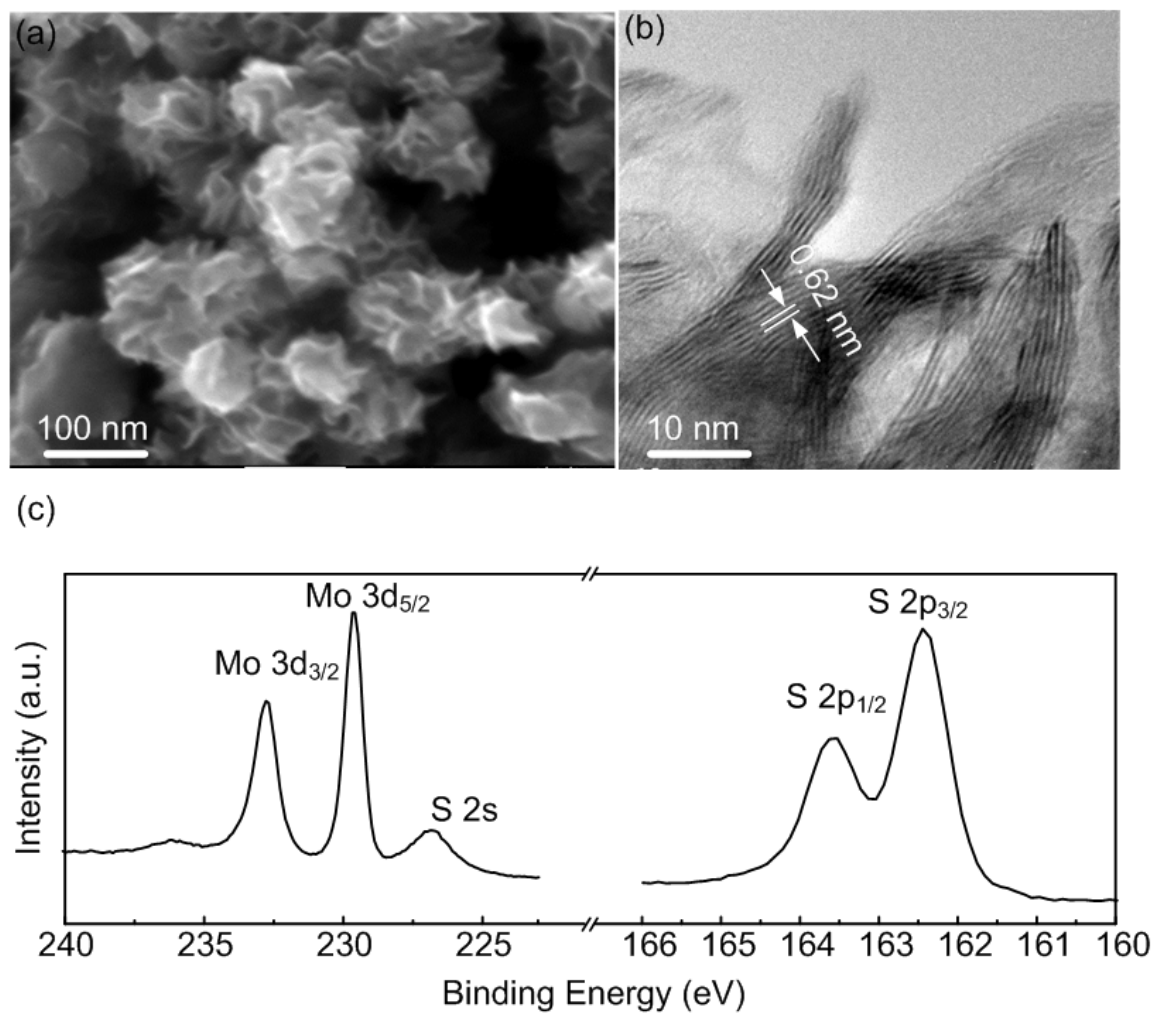


Figure 1. (a) SEM, (b) TEM images and (c) XPS core-level spectra of Mo 3d, S 2s and 2p of MoS₂/OLC nano-urchins.

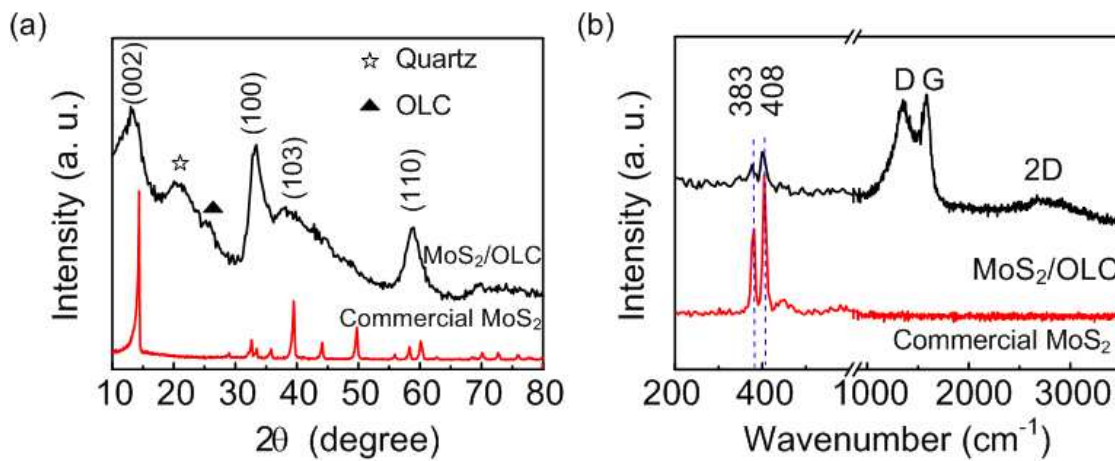


Figure 2. (a) XRD patterns and (b) Raman spectra of MoS₂/OLC nano-urchins and the commercial MoS₂ powders.

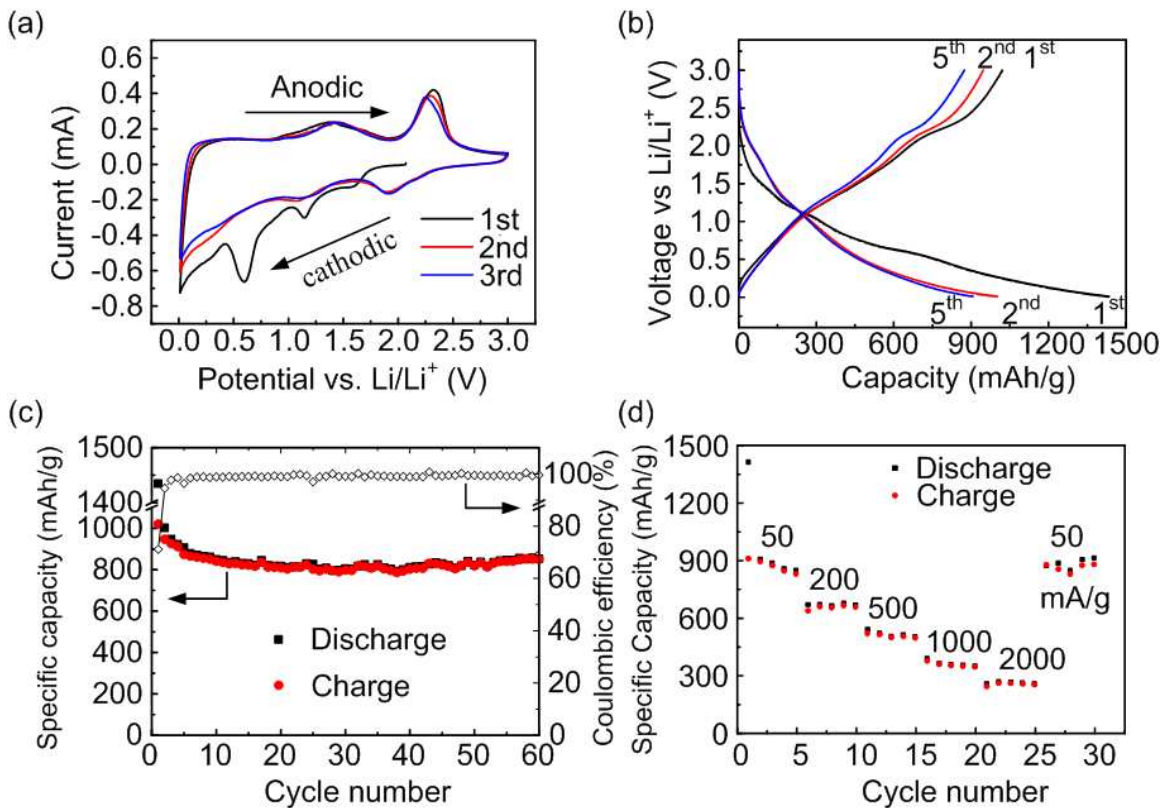


Figure 3. (a) Cyclic voltammetry (CV) curves of the MoS₂/OLC nano-urchins electrode of the first three cycles at a scan rate of 0.1 mV s⁻¹ in a potential range of 0.01–3 V vs. Li/Li⁺. (b) Galvanostatic discharge/charge curves of MoS₂/OLC nano-urchins electrode at a current density of 50 mA g⁻¹ for the first 5 cycles. (c) Cycling performance and related Coulombic efficiency of the MoS₂/OLC nano-urchins. (d) Rate capabilities of the MoS₂/OLC nano-urchins based electrodes.

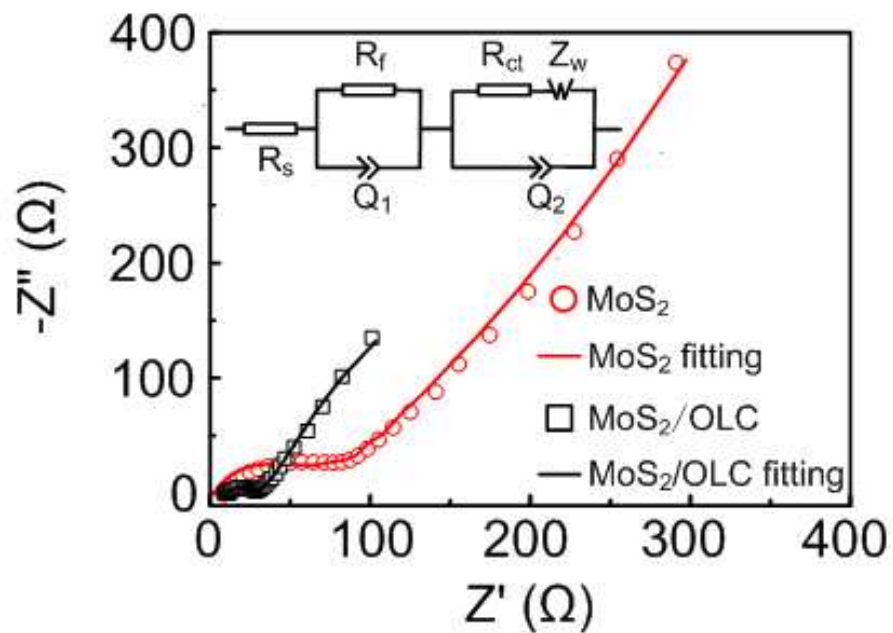


Figure 4. EIS spectra (symbol) and the corresponding fittings (solid line) of MoS₂/OLC nano-urchins and commercial MoS₂ powder electrodes. Inset shows the equivalent circuit model used for the fittings.

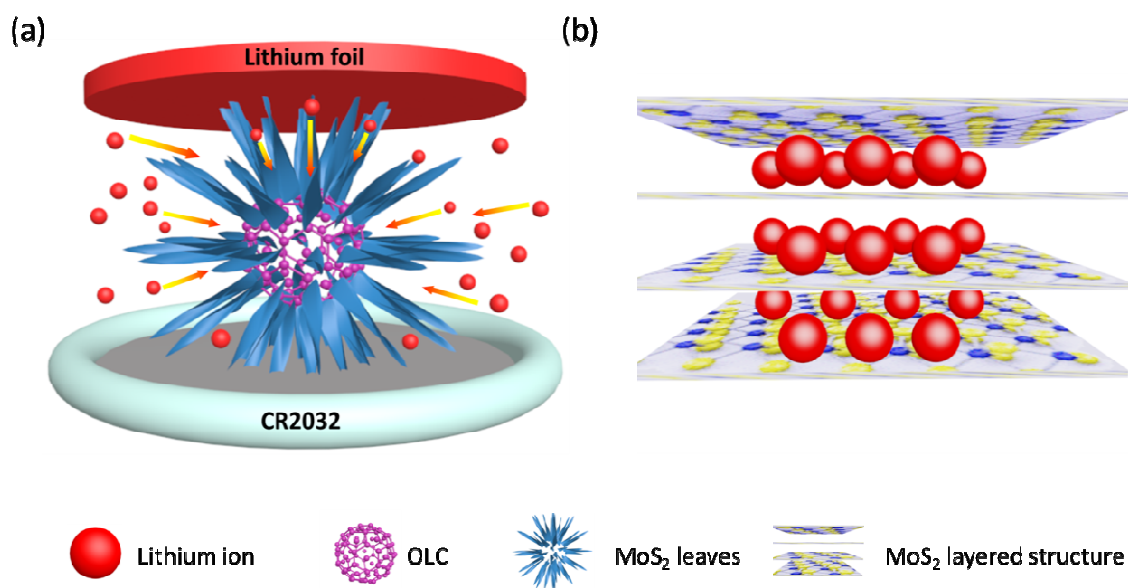


Figure 5. Schematic diagrams of (a) pre-lithiation process and device configuration and (b) MoS₂ layered structure with the intercalated lithium ions during the pre-lithiation process.

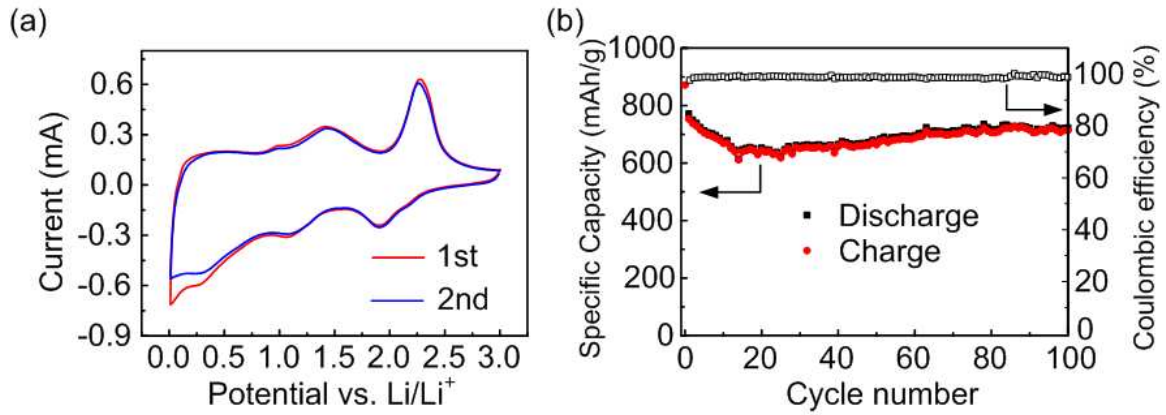


Figure 6. (a) CV and (b) cycling performance and related Coulombic efficiency of the pre-lithiated MoS₂/OLC nano-urchins at a current density of 50 mA g⁻¹.

Table 1. Fitting results of the EIS curves in **Figure 4** using the equivalent circuit.

Sample	Rs (Ω)	Rf (Ω)	Q1		Rct (Ω)	Q2		W (S.sec ⁵ /cm ²)	χ^2
			Y	n		Y	n		
MoS ₂	8.80	930.9	3.36E-3	0.80	60.62	1.60E-5	0.81	2.03E-3	5.35E-2
MoS ₂ /OLC	9.86	337.8	1.53E-2	0.97	19.22	4.00E-4	0.64	6.12E-2	1.59E-3